Advanced Structural Mechanics 1 (2022) 21-33

Advanced Structural Mechanics

journal homepage: http://asm.sku.ac.ir

Investigating the buckling and vibration of a Mindlin rectangular nanoplate using the modified couple stress theory

Majid Eskandari Shahraki [a, *], Mahmoud Shariati [b], Naser Asiaban [b], Ali Davar [c], Jafar Eskandari Jam [c], Mohsen Heydari Beni [c]

[a] *Department of Aerospace Engineering, Ferdowsi University of Mashhad, Mashhad, Iran*
[b] *Department of Mechanical Engineering, Ferdowsi University of Mashhad, Mashhad, Iran.*
[c] *Faculty of Materials and Manufacturing Technologies, Malek Ashtar University of Technology, Tehran, Iran*

Article received:2022/04/04, Article revised: 2022/05/02, Article accepted: 2022/09/08

ABSTRACT

This paper presents the buckling and vibration characteristics of a Mindlin rectangular nanoplate with simply supported boundary conditions and Navier approach. In order to consider the small scale effects, the modified couple stress theory with one length scale parameter is used. In the modified couple stress theory, the strain energy density is a function of strain tensor, curvature tensor, stress tensor, and symmetric part of the couple stress tensor. The critical buckling load values and vibration frequencies of different modes are separately solved. The governing equations are numerically solved and the results are verified with literature. The effect of material length scale, length, width and thickness of the nanoplate on the buckling loads and vibration frequencies are investigated and the results are presented and discussed in detail.

Keywords: Modified couple stress theory; Mindlin nanoplate; Buckling; Vibration; Navier's solution

1. Introduction

Performing experiments in the atomic and molecular scales is the safest approach for the study of materials in small-scales because the structures are investigated in real dimensions. In order to determine the mechanical properties of nanostructures in this method, various mechanical loads are applied on nanostructures using the atomic Force Microscopy (AFM) and the plate responses are measured. The difficulties with controlling the test conditions at this scale, high economic costs and time-consuming processes are some setbacks of this approach. Therefore, it is only used to validate other simple and low-cost methods.

Atomic simulation is another approach for studying small-scale structures. In this method, the behaviors of atoms and molecules are examined by considering the intermolecular and interatomic effects on their motions, which ultimately involves the total body deformation. In the case of large deformations and multi atomic scales, the computational costs of this approach become unbearable, so it is only used for small deformation problems.

Given the limitations of the aforementioned methods for the study of small-scales, many literatures have been directed toward finding more efficient solutions which are reliable, less costly, and time consuming. Modeling small-scale structures using continuum mechanics is one of these solutions. There are a variety of size-dependent continuum theories that take size effects into account and are suitable for this problem. Among these theories are micromorphic theory, microstructural theory, micropolar theory, Kurt's theory, non-local theory, modified couple stress theory, and strain gradient elasticity. Aghababaei and Reddy [1] employed the non-local third order shear deformation plate theory to study bending and vibration of plates. They presented Eringen's analytical solution for bending and free vibration of a simply supported rectangular plate using non-local linear elasticity theory to illustrate the effect of non-local theory on deflection and natural frequency of the plates. Shafiei et al. [2] employed the modified couple-stress theory to study stability and vibration of single and multi-layered graphene sheets. The effects of different parameters such as loading schemes, nanoplate dimensions, and boundary conditions were investigated.

* Corresponding author at: Department of Aerospace Engineering, Ferdowsi University of Mashhad, Mashhad, Iran.
E-mail address: mjdeskandari@gmail.com
DOI: 10.22034/asm.2022.13805.1001: http://asm.sku.ac.ir/article_11295.html

Sladek et al. [3] studied the FGM micro/nano-plates within the modified couple stress theory of elasticity. The boundary restrictions on the bottom and top surfaces of the plate together with derivation of governing equations and physical boundary conditions on the plate edges were investigated and discussed in detail. Thanh et al. [4] studied the size-dependent thermal bending and buckling responses of composite laminate microplate based on the new modified couple stress theory and isogeometric analysis. They also evaluated the impacts of fiber orientation, thickness ratio, boundary conditions, and variation in the material length scale parameter. Jung et al. [5] studied buckling of S-FGM nanoplates embedded in Pasternak elastic medium using the modified couple stress theory. The effects of power law index, small-scale coefficient, aspect ratio, side-to-thickness ratio, loading types, and elastic medium parameter on the buckling load of S-FGM nanoplates were also evaluated. Al-Shewailiah and Al-Shujairi [6] studied the static bending of functionally graded single-walled carbon nanotube conjunction using the modified couple stress theory. They investigated characteristics such as length, material parameter ratio, volume fraction of material, porosity and carbon nanotube, SWCNT distribution types, boundary conditions, and aspect ratio (length/thickness). By observing the static behavior of FG-micro beams it was found that the modified couple stress theory (MCST) yields more accurate results than classical beams. Yuan et al. [7] studied the couple stress-based nonlinear buckling of hydrostatic pressurized functionally graded composite conical microshells. They observed that the couple stress size dependency plays a more important role in the nonlinear buckling behavior of FG composite conical microshells. Kim et al. [8] studied the bending, free vibration, and buckling of the modified couples stress-based functionally graded porous micro-plates. They presented the numerical results of bending, free vibration, and buckling to determine the effects of constituent material variation, microstructure-dependent size effects, and porosity distributions on the mechanical response of functionally graded porous microplates.

In this paper, a Mindlin rectangular nanoplate model is developed for buckling and vibration analysis of a graphene nanoplate based on the modified couple stress theory. The results are presented in figures and tables and are discussed in detail.

2. Modified couple stress theory

In 2002, Yang et al. [9] proposed a modified couple stress model by modifying the theory proposed by Toppin [10], Mindlin and Tiersten [11], Koiter [12] and Mindlin [13] in 1964. The modified couple stress theory consists of one material length scale parameter for projection of the size effect, whereas the classical couple stress theory has two material length scale parameters. In the modified couple stress theory, the strain energy density in the three-dimensional vertical coordinates for a body bounded by the volume V and the area Ω [14] is expressed as follows Eq. (1):

$$U=\frac{1}{2}\int_V \left(\sigma_{ij}\varepsilon_{ij}+m_{ij}\chi_{ij}\right)dV \quad i,j=1,2,3 \tag{1}$$

where

$$\varepsilon_{ij}=\frac{1}{2}(u_{i,j}+u_{j,i}) \tag{2}$$

$$\chi_{ij}=\frac{1}{2}\left(\theta_{i,j}+\theta_{j,i}\right) \tag{3}$$

χ_{ij} and ε_{ij} are the symmetric parts of the curvature and strain tensors, respectively, and θ_i is the displacement vector and u_i denotes the rotational vector.

$$\theta=\frac{1}{2}\ \text{Curl u} \tag{4}$$

σ_{ij} the stress tensor, and m_{ij} the deviatoric part of the couple stress tensor, are defined as:

$$\sigma_{ij}=\lambda\varepsilon_{kk}\delta_{ij}+2\mu\varepsilon_{ij} \tag{5}$$

$$m_{ij}=2\mu\, l^2\chi_{ij} \tag{6}$$

where λ and μ are the lame constants, δ_{ij} is the Kronecker delta and l is the material length scale parameter. From Eqs. (3) and (6) it can be seen that χ_{ij} and m_{ij} are symmetric.

3. Mindlin's plate model

The displacement equations for the Mindlin's plate are defined as Eq. (7):

$$\begin{aligned} u_1\left(x,y,z,t\right)&=z\,\varphi_x(x,y,t)\\ u_2\left(x,y,z,t\right)&=z\,\varphi_y(x,y,t)\\ u_3\left(x,y,z,t\right)&=w\left(x,y,t\right)\end{aligned} \tag{7}$$

where φ_x and φ_y are the rotations of the normal vector around the x and y axis respectively, and w is the midpoint displacement of the plate in the z-axis direction.

In Fig.1. a Mindlin rectangular nanoplate with length a, width b, and thickness h is shown.

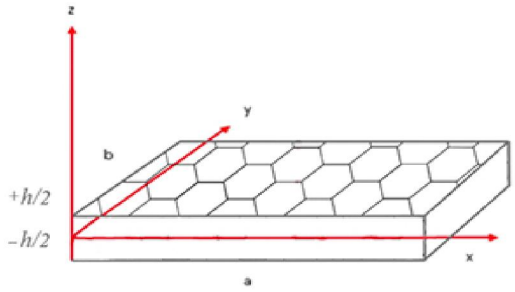

Fig.1. A schematic of the nanoplate and axes

The strain and stress tensors, symmetric part of the curvature tensor, and rotational vector for the Mindlin's plate are obtained as follows Eqs. (8-28):

$$\varepsilon_{xx}=z\frac{\partial\varphi_x}{\partial x} \tag{8}$$

$$\varepsilon_{yy}=z\frac{\partial\varphi_y}{\partial y} \tag{9}$$

$$\varepsilon_{zz}=0 \tag{10}$$

$$\varepsilon_{xy}=\varepsilon_{yx}=\frac{1}{2}z\left(\frac{\partial\varphi_x}{\partial y}+\frac{\partial\varphi_y}{\partial x}\right) \tag{11}$$

$$\varepsilon_{xz}=\varepsilon_{zx}=\frac{1}{2}\left(\frac{\partial w}{\partial x}+\varphi_x\right) \tag{12}$$

$$\varepsilon_{yz}=\varepsilon_{zy}=\frac{1}{2}\left(\frac{\partial w}{\partial y}+\varphi_y\right) \tag{13}$$

$$\theta_x=\frac{1}{2}\left(\frac{\partial w}{\partial y}-\varphi_y\right) \tag{14}$$

$$\theta_y=\frac{1}{2}\left(\varphi_x-\frac{\partial w}{\partial x}\right) \tag{15}$$

$$\theta_z=\frac{1}{2}z\left(\frac{\partial\varphi_y}{\partial x}-\frac{\partial\varphi_x}{\partial y}\right) \tag{16}$$

$$\chi_{xx}=\frac{1}{2}\left(\frac{\partial^2 w}{\partial x\,\partial y}-\frac{\partial\varphi_y}{\partial x}\right) \tag{17}$$

$$\chi_{yy}=\frac{1}{2}\left(\frac{\partial\varphi_x}{\partial y}-\frac{\partial^2 w}{\partial x\partial y}\right) \tag{18}$$

$$\chi_{zz}=\frac{1}{2}\left(\frac{\partial\varphi_y}{\partial x}-\frac{\partial\varphi_x}{\partial y}\right) \tag{19}$$

$$\chi_{xy}=\frac{1}{4}\left(\frac{\partial^2 w}{\partial y^2}-\frac{\partial^2 w}{\partial x^2}+\frac{\partial\varphi_x}{\partial x}-\frac{\partial\varphi_y}{\partial y}\right) \tag{20}$$

$$\chi_{xz}=\frac{1}{4}z\left(\frac{\partial^2\varphi_y}{\partial x^2}-\frac{\partial^2\varphi_x}{\partial y\,\partial x}\right) \tag{21}$$

$$\chi_{yz}=\frac{1}{4}z\left(\frac{\partial^2\varphi_y}{\partial x\partial y}-\frac{\partial^2\varphi_x}{\partial y^2}\right) \tag{22}$$

$$\sigma_{xx}=(\lambda+2\mu)\,z\frac{\partial\varphi_x}{\partial x}+\lambda z\frac{\partial\varphi_y}{\partial y} \tag{23}$$

$$\sigma_{yy}=\lambda z\frac{\partial \varphi_x}{\partial x}+(\lambda+2\mu)\, z\frac{\partial \varphi_y}{\partial y} \tag{24}$$

$$\sigma_{zz}=\lambda\left(z\frac{\partial \varphi_x}{\partial x}+z\frac{\partial \varphi_y}{\partial y}\right) \tag{25}$$

$$\sigma_{yx}=\sigma_{xy}=\mu z\left(\frac{\partial \varphi_x}{\partial y}+\frac{\partial \varphi_y}{\partial x}\right) \tag{26}$$

$$\sigma_{xz}=\sigma_{zx}=\mu\left(\frac{\partial w}{\partial x}+\varphi_x\right) \tag{27}$$

$$\sigma_{yz}=\sigma_{zy}=\mu\left(\frac{\partial w}{\partial y}+\varphi_y\right) \tag{28}$$

The variation of the strain energy is expressed as follows Eq. (29) :

$$\delta U=\int_V(\sigma_{xx}\,\delta\,\varepsilon_{xx}+\sigma_{yy}\,\delta\varepsilon_{yy}+2\sigma_{xy}\,\delta\,\varepsilon_{xy}+2\sigma_{xz}\,\delta\,\varepsilon_{xz}+2\sigma_{yz}\,\delta\,\varepsilon_{yz}+m_{xx}\delta x_{xx}+m_{yy}\,\delta x_{yy}+m_{zz}\,\delta x_{zz}+2m_{xy}\,\delta x_{xy}$$
$$+2m_{xz}\,\delta x_{xz}+2m_{yz}\,\delta\,x_{yz})\,dV \tag{29}$$

For the sake of simplification, the coefficient of each variable in the above equation is named from F_1 to F_{15} and this equation can be rewritten as shown below Eq. (30):

$$\delta U=\int_V(F_1\delta w,_{xx}+F_2\,\delta w,_{yy}+F_3\,\delta w,_{xy}+F_4\delta\, w,_x+F_5\,\delta\, w,_y+F_6\,\delta\,\varphi_{x,yy}+F_7\delta\,\varphi_{y,xx}+F_8\,\delta\,\varphi_{y,xy}+F_9\,\delta\varphi_{x,yx}+F_{10}\,\delta\,\varphi_{x,x}+$$
$$F_{11}\,\delta\varphi_{y,y}+F_{12}\delta\varphi_{x,y}+F_{13}\,\delta\,\varphi_{y,x}++F_{14}\,\delta\varphi_x+F_{15}\,\delta\varphi_y)dV \tag{30}$$

where

$$F_1=-\frac{1}{4}\mu l^2\left(\frac{\partial^2 w}{\partial y^2}-\frac{\partial^2 w}{\partial x^2}+\frac{\partial \varphi_x}{\partial x}-\frac{\partial \varphi_y}{\partial y}\right) \tag{31}$$

$$F_2=\frac{1}{4}\mu l^2\left(\frac{\partial^2 w}{\partial y^2}-\frac{\partial^2 w}{\partial x^2}+\frac{\partial \varphi_x}{\partial x}-\frac{\partial \varphi_y}{\partial y}\right) \tag{32}$$

$$F_3=\mu l^2\left(\frac{\partial^2 w}{\partial x\partial y}-\frac{1}{2}\frac{\partial \varphi_y}{\partial x}-\frac{1}{2}\frac{\partial \varphi_x}{\partial y}\right) \tag{33}$$

$$F_4=\mu\left(\frac{\partial w}{\partial x}+\varphi_x\right) \tag{34}$$

$$F_5=\mu\left(\frac{\partial w}{\partial y}+\varphi_y\right) \tag{35}$$

$$F_6=F_8=\frac{1}{4}\mu l^2 z^2\left(\frac{\partial^2 \varphi_y}{\partial x\partial y}-\frac{\partial^2 \varphi_x}{\partial y^2}\right) \tag{36}$$

$$F_7=F_9=\frac{1}{4}\mu l^2 z^2\left(\frac{\partial^2 \varphi_y}{\partial x^2}-\frac{\partial^2 \varphi_x}{\partial x\partial y}\right) \tag{37}$$

$$F_{10}=(\lambda+2\mu)\,z^2\frac{\partial \varphi_X}{\partial x}+\lambda z^2\frac{\partial \varphi_y}{\partial y}+\frac{1}{4}\mu l^2\left(\frac{\partial^2 w}{\partial y^2}-\frac{\partial^2 w}{\partial x^2}+\frac{\partial \varphi_x}{\partial x}-\frac{\partial \varphi_y}{\partial y}\right) \tag{38}$$

$$F_{11}=\lambda Z^2\frac{\partial \varphi_x}{\partial x}+(\lambda+2\mu)\,z^2\frac{\partial \varphi_y}{\partial y}-\frac{1}{4}\mu l^2\left(\frac{\partial^2 w}{\partial y^2}-\frac{\partial^2 w}{\partial x^2}+\frac{\partial \varphi_x}{\partial x}-\frac{\partial \varphi_y}{\partial y}\right) \tag{39}$$

$$F_{12}=\mu z^2\left(\frac{\partial \varphi_x}{\partial y}+\frac{\partial \varphi_y}{\partial x}\right)+\mu l^2\left(\frac{\partial \varphi_x}{\partial y}-\frac{1}{2}\frac{\partial \varphi_y}{\partial x}-\frac{1}{2}\frac{\partial^2 w}{\partial x\partial y}\right) \tag{40}$$

$$F_{13}=\mu z^2\left(\frac{\partial\varphi_x}{\partial y}+\frac{\partial\varphi_y}{\partial x}\right)+\mu l^2\left(\frac{\partial\varphi_y}{\partial x}-\frac{1}{2}\frac{\partial^2 w}{\partial x\partial y}-\frac{1}{2}\frac{\partial\varphi_x}{\partial y}\right) \tag{41}$$

$$F_{14}=\mu\left(\frac{\partial w}{\partial x}+\varphi_x\right) \tag{42}$$

$$F_{15}=\mu\left(\frac{\partial w}{\partial y}+\varphi_y\right) \tag{43}$$

4. The buckling load

For a rectangular plate with length a, width b, and thickness h, under the axial loads (P_{xy}, P_y, P_x), the buckling load is obtained as shown in Eq. (44) [15, 16]:

$$P_x\frac{\partial^2 w}{\partial x^2}+2P_{xy}\frac{\partial^2 w}{\partial x\partial y}+P_y\frac{\partial^2 w}{\partial y^2}=q(x,y) \tag{44}$$

where P_x is the axial load along the x axis, P_y is the axial load along the y axis, P_{xy} is the shear load in the xy plane, and $q\ (x, y)$ is the out-of-plane load.

5. Virtual work of the external loads

In this kind of problems, the virtual works of three kinds of external loads are included in the solutions, if the middle-plane and the middle-perimeter of the plate are shown as Ω and Γ, respectively, these virtual works are [17]:

1. The virtual work done by the body loads, which is applied on the volume $V=\Omega\times(-h/2, h/2)$.
2. The virtual work done by the surface tractions at the upper and lower surfaces (Ω).
3. The virtual work done by the shear tractions on the lateral surfaces, $S=\Gamma\times(-h/2, h/2)$.

If (f_x, f_y, f_z) are the body loads, (c_x, c_y, c_z) are the body couples, (q_x, q_y, q_z) are the loads acting on the Ω plane, (t_x, t_y, t_z) are the Cauchy's tractions and (S_x, S_y, S_z) are surface couples, then the variations of the virtual work is expressed as Eq. (45):

$$\delta w=-\left[\begin{array}{l}\int_\Omega (f_x\delta u+f_y\delta V+f_z\delta w+q_x\delta u+q_y\delta V+q_z\delta w+c_x\delta q_x+c_y\delta q_y+c_z\delta q_z)dx\,dy+\\ \int_\Gamma (t_x\delta u+t_y\delta V+t_z\delta w+s_x\delta q_x+s_y\delta q_y+s_z\delta q_z)d\Gamma\end{array}\right] \tag{45}$$

Given that in this study only the external load q_z was applied, virtual work becomes Eq. (46):

$$\delta w=\int_0^a\int_0^b q(x,y)\,\delta w(x,y)\,dx\,dy \tag{46}$$

The variation of kinetic energy is obtained as Eq. (47) :

$$\delta T=\int_A\int_{-\frac{h}{2}}^{\frac{h}{2}}\rho\left(\dot u_1\delta\dot u_1+\dot u_2\delta\dot u_2+\dot u_3\delta\dot u_3\right)dA\,dz=\int_A\left[\rho h\dot w\delta\dot w+\frac{\rho h^3}{12}\left(\dot\varphi_x\delta\dot\varphi_x+\dot\varphi_y\delta\dot\varphi_y\right)\right]dA \tag{47}$$

where ρ is the density.

Finally, using Hamilton's principle, it can be said that [16]:

$$\int_0^T\left(\delta T-\left(\delta U-\delta w\right)\right)dt=0 \tag{48}$$

where T is the kinetic energy, U is the strain energy, and W is the work of the external loads.

6. The final governing equations of the plate after applying the buckling and external loads

Using Hamilton's principle, the Eq. (48), and the Eqs. (44) -(47), the governing equations of the plate, including the buckling and external loads, are obtained as follows Eqs. (49-51):

$$\left[\int_{-h/2}^{h/2}\left(\frac{\partial^2 F_1}{\partial x^2}-\frac{\partial F_4}{\partial x}+\frac{\partial^2 F_2}{\partial y^2}+\frac{\partial^2 F_3}{\partial x\partial y}-\frac{\partial F_5}{\partial y}\right)dz\right]=q(x,y)+\rho h\frac{\partial^2 w}{\partial t^2} \tag{49}$$

$$\int_{-h/2}^{h/2}\left(\frac{\partial^2 F_6}{\partial y^2}+\frac{\partial^2 F_9}{\partial x\partial y}-\frac{\partial F_{12}}{\partial y}-\frac{\partial F_{10}}{\partial x}+F_{14}\right)dz=\frac{\rho h^3}{12}\frac{\partial^2\varphi_x}{\partial t^2} \tag{50}$$

$$\int_{-h/2}^{h/2}\left(\frac{\partial^2 F_7}{\partial x^2}-\frac{\partial F_{13}}{\partial x}+\frac{\partial^2 F_8}{\partial x\partial y}-\frac{\partial F_{11}}{\partial y}+F_{15}\right)dz=\frac{\rho h^3}{12}\frac{\partial^2\varphi_y}{\partial t^2} \tag{51}$$

7. Obtaining the general governing equation of the Mindlin's plate

Considering the following constants Eqs. (52-60):

$$C_1=\frac{1}{4}\mu l^2 h \tag{52}$$

$$C_2=\mu h\, k_s \tag{53}$$

$$C_3=\frac{1}{4}\mu l^2 I_2 \tag{54}$$

$$C_4=-\mu I_2-\mu l^2 h \tag{55}$$

$$C_5=-\lambda I_2-2\mu I_2-\frac{1}{4}\mu l^2 h \tag{56}$$

$$C_6=-\mu I_2-\lambda I_2+\frac{3}{4}\mu l^2 h \tag{57}$$

$$C_7=\rho h \tag{58}$$

$$C_8=\frac{\rho h^3}{12} \tag{59}$$

$$k_s=\frac{5}{6}=0.8 \tag{60}$$

where,

$$I_i=\int_{-\frac{h}{2}}^{\frac{h}{2}} Z^i\ dz \tag{61}$$

the general governing equation of the Mindlin's plate will become Eqs. (62-64):

$$\begin{aligned}&2C_1\frac{\partial^4 w}{\partial x^2\partial y^2}+C_1\frac{\partial^4 w}{\partial x^4}+C_1\frac{\partial^4 w}{\partial y^4}-C_2\frac{\partial^2 w}{\partial x^2}-C_2\frac{\partial^2 w}{\partial y^2}-C_1\frac{\partial^3\varphi_x}{\partial x^3}-C_1\frac{\partial^3\varphi_y}{\partial y^3}-C_1\frac{\partial^3\varphi_x}{\partial x\,\partial y^2}\\&-C_1\frac{\partial^3\varphi_y}{\partial x^2\partial y}-C_2\frac{\partial\varphi_x}{\partial x}-C_2\frac{\partial\varphi_y}{\partial y}+P_x\frac{\partial^2 w}{\partial x^2}+2P_{xy}\frac{\partial^2 w}{\partial x\,\partial y}+P_y\frac{\partial^2 w}{\partial y^2}=q(x,y)+C_7\frac{\partial^2 w}{\partial t^2}\end{aligned} \tag{62}$$

$$C_3\left(\frac{\partial^4\varphi_y}{\partial x\,\partial y^3}-\frac{\partial^4\varphi_x}{\partial y^4}+\frac{\partial^4\varphi_y}{\partial x^3\partial y}-\frac{\partial^4\varphi_x}{\partial x^2\partial y^2}\right)+C_4\frac{\partial^2\varphi_x}{\partial y^2}+C_5\frac{\partial^2\varphi_x}{\partial x^2}+C_6\frac{\partial^2\varphi_y}{\partial x\,\partial y}+C_1\frac{\partial^3 w}{\partial x\,\partial y^2}+C_1\frac{\partial^3 w}{\partial x^3}+C_2\frac{\partial w}{\partial x}+C_2\varphi_x=C_8\frac{\partial^2\varphi_x}{\partial t^2} \tag{63}$$

$$C_3\left(\frac{\partial^4\varphi_y}{\partial x^4}-\frac{\partial^4\varphi_x}{\partial x^3\partial y}+\frac{\partial^4\varphi_y}{\partial x^2\partial y^2}-\frac{\partial^4\varphi_x}{\partial x\,\partial y^3}\right)+C_6\frac{\partial^2\varphi_x}{\partial x\,\partial y}+C_4\frac{\partial^2\varphi_y}{\partial x^2}+C_5\frac{\partial^2\varphi_y}{\partial y^2}+C_1\frac{\partial^3 w}{\partial y\,\partial x^2}+C_1\frac{\partial^3 w}{\partial y^3}+C_2\frac{\partial w}{\partial y}+C_2\varphi_x=C_8\frac{\partial^2\varphi_y}{\partial t^2} \tag{64}$$

8. Solution of the governing equations using Navier's method

The Navier's solution is applicable to the rectangular plates which simply support the boundary conditions on all edges. Since the boundary conditions are spontaneously satisfied in this method, the unknown functions of the plate's mid-plane are assumed to be double trigonometric series [15, 17]:

$$W(x,y,t)=\sum_{m=1}^{\infty}\sum_{n=1}^{\infty}W_{mn}\sin\alpha x\sin\beta y\, e^{i\omega t} \tag{65}$$

$$\varphi_x(x,y,t)=\sum_{m=1}^{\infty}\sum_{n=1}^{\infty}X_{mn}\cos\alpha x\sin\beta y\, e^{i\omega t} \tag{66}$$

$$\varphi_y(x,y,t)=\sum_{m=1}^{\infty}\sum_{n=1}^{\infty}y_{mn}\sin\alpha x\cos\beta y\, e^{i\omega t} \tag{67}$$

the load can also be calculated from the following relations Eqs. (68-70):

$$q=\sum_{m=1}^{\infty}\sum_{n=1}^{\infty}Q_{mn}\sin\alpha x\sin\beta y\, e^{i\omega t} \tag{68}$$

$$Q_{mn}=\frac{4}{ab}\int_0^a\int_0^b q(x,y)\sin\alpha x\sin\beta y\, dx\, dy \tag{69}$$

$$Q_{mn}=\begin{cases} q_0 & ;\text{For sinusoidal load}\\ \dfrac{16q_0}{mn\pi^2} & ;\text{For uniform load}\\ \dfrac{4Q_0}{ab} & ;\text{For point load in the plane center}\end{cases} \tag{70}$$

where

$$\alpha=\frac{\pi m}{a}\ ,\ \beta=\frac{\pi n}{b}\ ,\ i=\sqrt{-1} \tag{71}$$

Simply-supported boundary conditions are also satisfied by the Navier's method according to the following Eqs. (72-73):

$$\begin{cases} x=0 \\ x=a \end{cases}\ ,\ \begin{cases} w(0,y)=w(a,y)=\sum\sum w_{mn}\sin\dfrac{m\pi}{a}\,x\sin\dfrac{n\pi}{b}\,y=0 \\ \varphi_y(0,y)=\varphi_y(a,y)=\sum\sum y_{mn}\sin\dfrac{m\pi}{a}\,x\cos\dfrac{n\pi}{b}\,y=0 \end{cases} \tag{72}$$

$$\begin{cases} y=0 \\ y=b \end{cases}\ ,\ \begin{cases} w(x,0)=w(x,b)=\sum\sum w_{mn}\sin\dfrac{m\pi}{a}\,x\sin\dfrac{n\pi}{b}\,y=0 \\ \varphi_x(x,0)=\varphi_x(x,b)=\sum\sum X_{mn}\cos\dfrac{m\pi}{a}\,x\sin\dfrac{n\pi}{b}\,y=0 \end{cases} \tag{73}$$

9. The general equation matrix of a Mindlin's plate

After solving the governing equations and naming the coefficient of each variable, we have:

$$U_1=2C_1\alpha^2\beta^2+C_1\alpha^4+C_1\beta^4+C_2\alpha^2+C_2\beta^2-P_x\alpha^2-P_y\beta^2 \tag{74}$$

$$U_2=U_4=-C_1\alpha^3-C_1\alpha\beta^2+C_2\alpha \tag{75}$$

$$U_3=U_7=-C_1\beta^3-C_1\alpha^2\beta+C_2\beta \tag{76}$$

$$U_5=-C_3\beta^4-C_3\alpha^2\beta^2-C_4\beta^2-C_5\alpha^2+C_2 \tag{77}$$

$$U_6=C_3\alpha\beta^3+C_3\alpha^3\beta-C_6\alpha\beta \tag{78}$$

$$U_8=-C_3\alpha^3\beta-C_3\alpha\beta^3-C_6\alpha\beta \tag{79}$$

$$U_9=C_3\alpha^4+C_3\alpha^2\beta^2-C_4\alpha^2-C_5\beta^2+C_2 \tag{80}$$

$$K_1=-C_7 \tag{81}$$

$$K_2=K_3=K_4=K_6=K_7=K_8=0 \tag{82}$$

$$K_5=K_9=-C_8 \tag{83}$$

Finally, the general equation matrix of the Mindlin's plate along with the auxiliary equations are obtained as follows Eq. (84):

$$\left(\begin{bmatrix} U_1 & U_2 & U_3 \\ U_4 & U_5 & U_6 \\ U_7 & U_8 & U_9 \end{bmatrix} - \omega^2 \begin{bmatrix} K_1 & K_2 & K_3 \\ K_4 & K_5 & K_6 \\ K_7 & K_8 & K_9 \end{bmatrix}\right)\begin{bmatrix} w_{mn} \\ X_{mn} \\ y_{mn} \end{bmatrix} = \begin{bmatrix} Q_{mn} \\ 0 \\ 0 \end{bmatrix} \tag{84}$$

Various materials such as epoxy, graphene, copper etc., can be considered as the plate's material. In this study, graphene is chosen as the plate's material. A single-layer graphene plate has the following properties [18]:

$E=1.06TPa$, $\nu=0.25$, $h=0.34nm$, $\rho=2250\ kg/m^3$

Moreover, the relationship between E, μ, and ν can be expressed as:

$$\lambda=\frac{\nu E}{(1+\nu)(1-2\nu)}\ ,\ \mu=\frac{E}{2(1+\nu)} \tag{85}$$

where μ and λ are the lame's coefficients and E is the Young's modulus [19]. The value of the distributed load is considered to be $q = 1N/m^2$.

10. Results and Discussion

Results were obtained using a computational program coded in the MATLAB software. The obtained results were compared with the literature [20,21] and good agreements between the overall results process were observed. The plate's dimensional parameters are chosen as follows:

a: plate's length
b: plate's width
h: plate's thickness
l: material length scale parameter

Table 1 compares the values of dimensionless critical load for different nanoplates under a bi-axial surface loading in x & y directions. By increasing the plate's length to thickness ratios, it is observed that:

- The value of dimensionless critical load for Mindlin nanoplates increases.
- The value of dimensionless critical load for 3rd and 5th order shear deformation nanoplate slightly decreases.
- The value of dimensionless critical load for Kirchhoff nanoplate remains unchanged.

Figure 2 compares the values of critical load of different nanoplates under the uniform surface traction for different length to thickness ratios. As can be seen, the 3rd order shear deformation nanoplate yielded the lowest values and the Mindlin nanoplate yielded the highest values for critical load.

Table 2 shows that the value of critical load for Mindlin's nanoplate under a bi-axial surface load in x and y directions increases due to an increase in the length scale parameter to thickness and decreases due to an increase in the length to thickness ratio of the nanoplate.

Figure 3 shows the value of dimensionless critical load for Mindlin's nanoplate under a uniaxial load in the x-direction. It was found that this value increases due to an increase in the length to thickness ratio of the nanoplate. Furthermore, when the effect of size parameter is neglected (classical theory), the value of dimensionless critical load becomes constant and reaches its lowest value, but with an increase in the size parameter, the dimensionless critical load value increases.

Figure 4 shows the value of dimensionless critical load for Mindlin's nanoplate under a biaxial surface load in x and y directions in different modes. As can be seen, this value increases due to an increase in the length scale parameter to thickness ratio of nanoplate. Furthermore, the first mode has the highest dimensionless critical load value, but this value gradually decreases for the next modes.

Figures 5-8 show the frequency of different modes of Mindlin's nanoplate ($\omega_{11} - \omega_{12} - \omega_{21} - \omega_{22}$). It is observed that this value decreases due to an increase in the length to thickness ratio. Moreover, for classical theory (by neglecting the effect of size parameter), the frequency reaches its lowest value, but the frequency values increase with an increase in the size effect. Furthermore, it is shown that the first mode has the lowest frequency and it increases for the next modes.

Table 1. Values of the dimensionless critical load of buckling for different nanoplates under a bi-axial surface loading for various length to thickness ratios (*l/h= , a/b=1, Py/Px=1).*

a/h	Kirchhoff plate	Mindlin plate	Third order shear deformation plate	N order shear deformation plate (*n=5*)
5	5.0000	10.1594	5.6521	5.6937
10	5.0000	12.8101	5.1723	5.1826
20	5.0000	13.6820	5.0437	5.0463
30	5.0000	13.8568	5.0195	5.0206
40	5.0000	13.9191	5.0110	5.0116
50	5.0000	13.9481	5.0070	5.0074

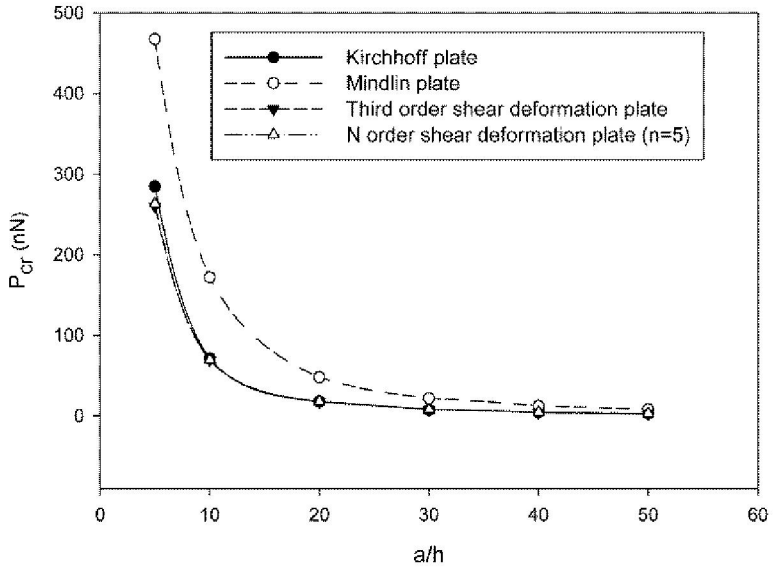

Fig. 2. Comparison of the critical load values for different nanoplates under the uniform surface traction in x direction for different length to thickness ratios (*a/b=1, l/h=1*).

Table 2. The comparison of buckling values of the Mindlin's nanoplate under biaxial loads for various length to thickness ratios (*Py/Px=1, a/b=1).*

a/h	l/h				
	0	0.5	1	1.5	2
10	6.7163	28.2488	86.0362	162.1843	233.7019
20	1.7526	7.4278	23.9784	50.02999	83.4495
30	0.7853	3.3333	10.8814	23.1469	39.6731
40	0.4430	1.8814	6.1660	13.2059	22.8526
50	0.2839	1.2060	3.9597	8.5076	14.7879

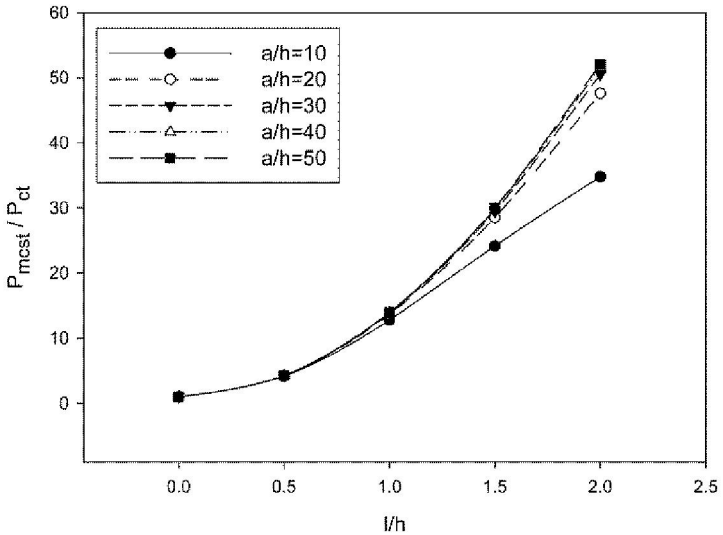

Fig. 3. Values of dimensionless critical load for Mindlin's nanoplate under a uniaxial load in the x-direction for different material length scale to thickness ratios and length to thickness ratio of the nanoplate (*a/b=1*).

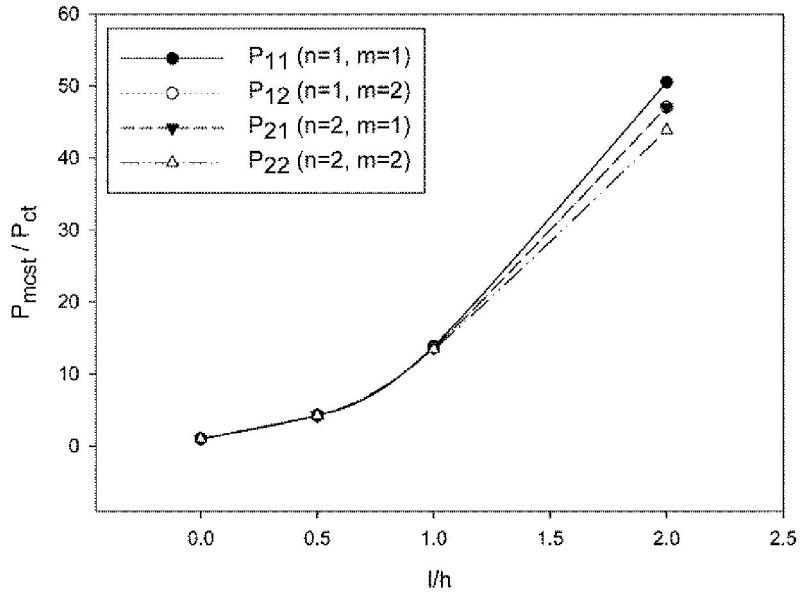

Fig. 4. Values of dimensionless critical load for Mindlin's nanoplate under a bi-axial surface load in *x* and *y* directions for material length scale to thickness ratio of the nanoplate (*a/b=1, a/h=30*).

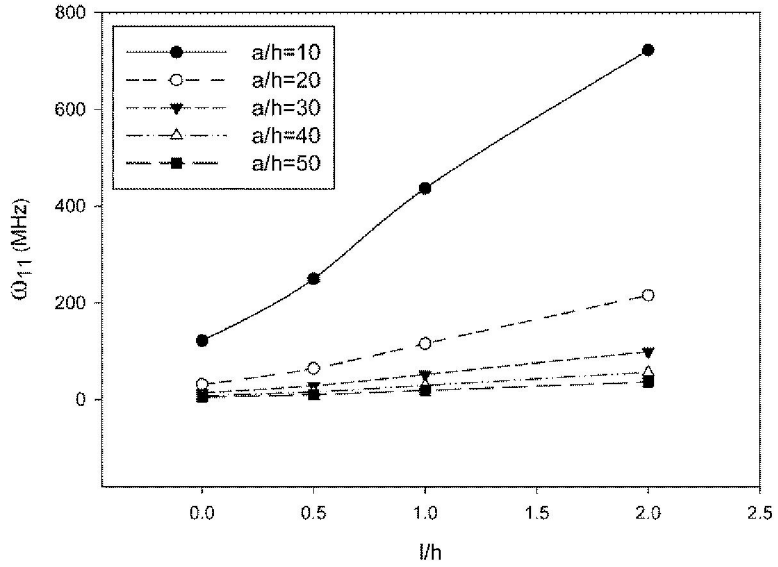

Fig. 5. Comparison of frequencies of the first mode (ω_{11}) for a Mindlin's nanoplate for various material length scale parameter to thickness and length to thickness ratios of the nanoplate (*a/b=1, h=0.34*).

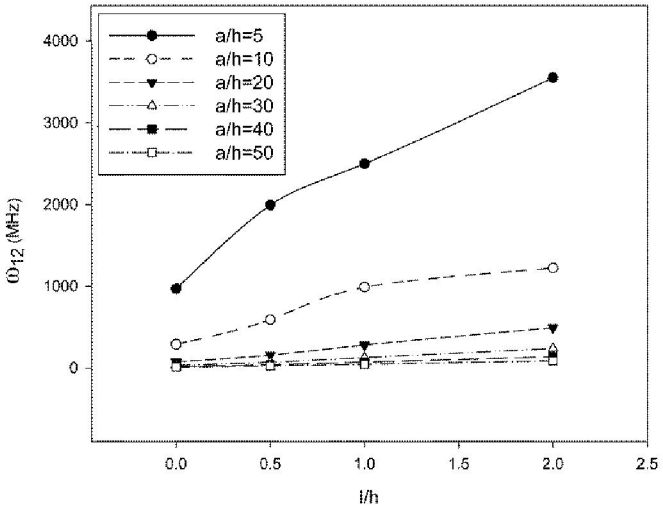

Fig. 6 Comparison of frequencies of the mode (ω_{12}) for a Mindlin's nanoplate for different material length scale parameter to thickness ratios ($a/b=1$, $h=0.34$).

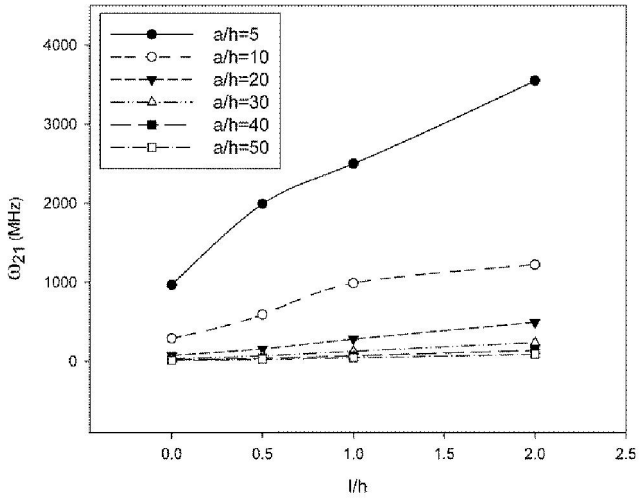

Fig. 7. Comparison of frequencies of the mode (ω_{21}) for a Mindlin's nanoplate for different material length scale parameter to thickness ratios ($a/b=1$, $h=0.34$).

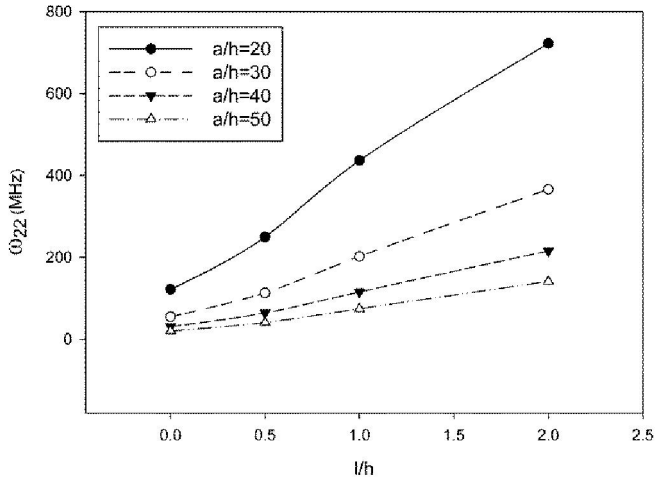

Fig. 8 Comparison of frequencies of the mode (ω_{22}) for a Mindlin's nanoplate for different material length scale parameter to thickness ratios ($a/b=1$, $h=0.34$).

As shown in Table 3 by increasing the aspect ratio of the nanoplate, the vibration frequency value decreases.

Table 4 shows the frequencies of various nanoplates at different vibration modes($\omega_{11} - \omega_{12} - \omega_{21} - \omega_{22}$). According to the Table, the Kirchhoff's nanoplate yields the highest frequency value when the length scale parameter is neglected, but the Mindlin's nanoplate yields the highest frequency value when the length scale parameter is considered.

Table 3. Comparison of different modes of frequency for Mindlin nanoplate for various length to thickness and aspect ratios (*l/h=1).*

Mode	a/h			
	20	30	40	50
	a/b=0.5			
ω_{11}	280.4153	128.0217	72.7219	46.7575
ω_{12}	436.5378	202.1703	115.4757	74.4444
ω_{21}	860.2980	413.9252	240.0504	155.9272
ω_{22}	988.5087	481.2484	280.4153	182.5827
	a/b=1			
ω_{11}	115.4757	51.9052	29.3145	18.7965
ω_{12}	280.4153	128.0217	72.7219	46.7575
ω_{21}	280.4153	128.0217	72.7219	46.7575
ω_{22}	436.5378	202.1703	115.4757	74.4444
	a/b=1.5			
ω_{11}	83.8680	37.5829	21.2022	13.5879
ω_{12}	159.1488	071.8354	40.6324	26.0724
ω_{21}	250.5691	114.0783	64.7336	41.6004
ω_{22}	321.6951	147.4292	83.8680	53.9616

Table 4. Comparison of dimensionless frequencies of different modes of various nanoplates for length to thickness ratio (*a/b=2, a/h=30).*

Mode	l/h			
	0	0.5	1	2
	Mindlin plate			
ω_{11}	8.7280	17.9862	32.5528	62.6001
ω_{12}	13.9429	28.7266	051.9052	99.1252
ω_{21}	29.4914	60.7224	109.1821	204.2795
ω_{22}	34.6425	71.3140	128.0217	237.9174
	Kirchhoff plate			
ω_{11}	8.7459	12.3685	19.5563	36.0601
ω_{12}	13.9886	19.7828	31.2794	57.6764
ω_{21}	29.6953	41.9954	66.4006	122.4367
ω_{22}	34.9237	49.3895	78.0917	143.9940
	Third order shear deformation plate			
ω_{11}	8.7284	12.3536	19.5411	36.0389
ω_{12}	13.9441	19.7447	31.2407	57.6223
ω_{21}	29.4967	41.8251	66.2277	122.1954
ω_{22}	34.6497	49.1546	77.8533	143.6613

11. Conclusion

In this study, the buckling and vibration of a Mindlin's nanoplate were investigated using the modified couple stress theory. As shown in the tables and figures, under an axial load, the minimum and maximum buckling critical load is observed for the third order shear deformation nanoplate and the Mindlin's nanoplate, respectively. Moreover, under a biaxial loading, buckling critical load increases due to an increase in material length scale parameter to thickness ratio and decreases due to an increase in the length to thickness ratio of the nanoplate.

It was found that the frequencies of different modes of Mindlin nanoplate decrease due to an increase in the length to thickness ratio. In addition, the frequency reaches its lowest value for classical theory (by neglecting the effect of size parameter), but the frequency values increase with an increase in the size effect. It was also found that the first mode yields the lowest frequency value but it increases for the next modes. Finally, it was seen that the vibration frequency decreases due to an increase in the plate's aspect ratio.

References

[1] Aghababaei, R., Reddy, J.N., 2009. Nonlocal third-order shear deformation plate theory with application to bending and vibration of plates. Journal of Sound and Vibration. 326, 277-289.

[2] Shafiei, Z., Sarrami-Foroushani, S., Azhari, F., Azhari, M., 2020. Application of modified couple-stress theory to stability and free vibration analysis of single and multi-layered graphene sheets. Aerospace Science and Technology. 98, 105652.

[3] Sladek, V., Sladek, J., Repka, M., Sator, L., 2020. FGM micro/nano-plates within modified couple stress elasticity. Composite Structures. 245, 112294.

[4] Thanh, C.L., Tran, L.V., Vu-Huu, T., Abdel-Wahab, M., 2019. The size-dependent thermal bending and buckling analyses of composite laminate microplate based on new modified couple stress theory and isogeometric analysis. Computer Methods in Applied Mechanics and Engineering. 350, 337-361.

[5] Jung, W.Y., Han, S.C., Park, W.T., 2014. A modified couple stress theory for buckling analysis of S-FGM nanoplates embedded in Pasternak elastic medium. Composites Part B: Engineering. 60, 746-756.

[6] Al-Shewailiah, D.M.R., Al-Shujairi, M.A., 2022. Static bending of functionally graded single-walled carbon nanotube conjunction with modified couple stress theory. Materials Today: Proceedings. 61, 1023–1037.

[7] Yuan, Y., Zhao, K., Zhao, Y., Sahmani, S., Safaei, B., 2020. Couple stress-based nonlinear buckling analysis of hydrostatic pressurized functionally graded composite conical microshells. Mechanics of Materials. 148, 103507.

[8] Kim, J., Żur, K.K., Reddy, J.N., 2019. Bending, free vibration, and buckling of modified couples stress-based functionally graded porous micro-plates. Composite Structures. 209, 879-888.

[9] Yang, F., Chong, A.C.M., Lam, D.C.C., Tong, P., 2002. Couple stress Based Strain gradient theory for elasticity. International Journal of Solids and Structures.39, 2731–2743.

[10] Toupin, R.A., 1962. Elastic materials with couple stresses. Archive for Rational Mechanics and Analysis. 11, 385–414.

[11] Mindlin, R.D., Tiersten, H.F., 1962. Effects of couple-stresses in linear elasticity. Archive for Rational Mechanics and Analysis. 11, 415–448.

[12] Koiter, W.T., 1964. Couple stresses in the theory of elasticity. Proceedings of the Koninklijke Nederlandse Akademie van Wetenschappen. (B) .67, 17–44.

[13] Mindlin, R.D., 1964. Micro-structure in linear elasticity. Archive for Rational Mechanics and Analysis. 16, 51–78.

[14] Tsiatas, G.C., 2009. A new Kirchhoff model based on a modified couple stress theory. International Journal of solids and structures. 46, 2757-2764.

[15] Wang, B., Zhou, S., Zhao, J., Chen, X., 2011. Asize-dependent Kirchhoff micro-plate model based on strain gradient elasticity theory. European Journal of mechanics A/Solids. 30, 517-524.

[16] Farajpour, A., Shahidi, A.R., Mohammadi, M., Mahzoon, M., 2012. Buckling of orthotropic micro/nanoscale plates under linearly varying in-plane load via nonlocal continuum mechanics. Composite Structures. 94, 1605-1615.

[17] Thai, H.T., Choi, D.H., 2013. size-dependent functionally graded Kirchhoff and Mindlin plate theory based on a modified couple stress theory. Composite Structures. 95, 142-153.

[18] Akgoz, B., Civalek, O., 2012. Free vibration analysis for single –layered graphene sheets in an elastic matrix via modified couple stress theory. Materials and Design. 42, 164-171.

[19] Roque, C.M.C., Ferreira, A.J.M., Reddy, J.N., 2013. Analysis of Mindlin micro plates with a modified couple stress theory and meshlessmethod. Applied Mathematical Modeling. 37, 4626-4633.

[20] Zhang, B., He, Y., Liu, D., Shen, L., Lei, J., 2015. An efficient size-dependent plate theory for bending, buckling and free vibration analyses of functionally graded microplates resting on elastic foundation. Applied Mathematical Modelling. 39, 3814–3845.

[21] Jung, W.Y., Han, S.C., Park, W.T., 2014. A modified couple stress theory for buckling analysis of S-FGM nanoplates embedded in Pasternak elastic medium. Composites Part B: Engineering. 60, 746-756.